

# Photonic gaps in cholesteric elastomers under deformation

P. Cicuta,<sup>1,2</sup> A.R. Tajbakhsh,<sup>1</sup> and E.M. Terentjev<sup>1</sup>

<sup>1</sup>*Cavendish Laboratory, University of Cambridge, Madingley Road, Cambridge, CB3 0HE, U.K.*

<sup>2</sup>*Nanoscience Center, University of Cambridge, J.J.Thomson Avenue, Cambridge, CB3 0FF, U.K.*

Cholesteric liquid crystal elastomers have interesting and potentially very useful photonic properties. In an ideal monodomain configuration of these materials, one finds a Bragg-reflection of light in a narrow wavelength range and a particular circular polarization. This is due to the periodic structure of the material along one dimension. In many practical cases, the cholesteric rubber possesses a sufficient degree of quenched disorder, which makes the selective reflection broadband. We investigate experimentally the problem of how the transmittance of light is affected by mechanical deformation of the elastomer, and the relation to changes in liquid crystalline structure. We explore a series of samples which have been synthesized with photonic stop-gaps across the visible range. This allows us to compare results with detailed theoretical predictions regarding the evolution of stop-gaps in cholesteric elastomers.

PACS numbers: 61.41.+e, 42.70.Qs, 83.80.Xz

## I. INTRODUCTION

In liquid crystal elastomers, the rubbery polymer network is made of chains that include rod-like mesogenic units as sections of the main chain or as side chains. The physical properties and the response of these materials to external fields are extremely rich and lead to a variety of applications. Experiments and theoretical studies in this field have been carried out by a number of groups for some time and this topic is broadly reviewed in the recent monograph [1].

A cholesteric (chiral nematic) phase can be induced in a nematic liquid crystal by adding of small quantity of chiral molecules, called the chiral dopant in this context. In an ideal cholesteric elastomer (CLCE) the liquid crystal structure is locally nematic, and a director can be identified in each  $x$ - $y$  plane forming an angle  $\phi$  to the  $x$  axis [2]. The director rotates continuously as a function of  $z$ , see Fig. 1, forming a periodic helical structure characterized by a pitch  $p$  (or equivalently by the wave number  $q = 2\pi/p$ ). Because of the local quadrupolar symmetry of the nematic order, the periodicity interval along  $z$  is only  $p/2$ . Cholesteric liquid crystals have complex optical properties due to their high local birefringence and the modulation on the length scale  $p$ , often comparable with the wavelength of light [3]. For example, circularly polarized light with wavelength  $\Lambda_0$  incident on the sample will not be transmitted if its handedness is the same as the cholesteric helix and its wavelength is  $\Lambda_0 = p\bar{m}$ , where  $\bar{m} = \frac{1}{2}(m_o + m_e)$  and  $m_o$  and  $m_e$  are the indexes of refraction of the liquid crystal. This determines a photonic stop-band, that is a 1D-bandgap, for a narrow range of wavelengths and one circular polarization of light. Furthermore, linearly polarized light on either side of the bandgap is very strongly rotated.

The study of advanced optical properties of CLCE has only become possible recently, in spite of the fact that the materials were first synthesized a long time ago [4]. The breakthrough has been achieved by Kim and Finkelmann [5], who developed a technique of forming monodomain

cholesteric structures crosslinked into the rubbery network; in most other circumstances a network ends up polydomain, with strong quenched disorder – it scatters light and is not useful for any optical purpose. Advantages of having a well-ordered material with a photonic stop-gap that can be altered by mechanical deformation of the rubber have been demonstrated by, e.g. the use of CLCE as cavities in tunable lasers [6]. Further applications will emerge as the surprising properties of these materials become better known.

In recent work [7] we have studied the elastic behavior of a monodomain CLCE and its relation to the underlying structure, through a combination of structural (X-ray) and mechanical probes. Optical investigation was also employed to provide precise measurements of the sample deformation. In brief, the behavior under uniaxial strain is complex, because the director tends to align along the stress axis but this is resisted by the anchoring of the local director to the initial crosslinked helical texture. Theoretical analysis [8] predicts in detail how the ideal cholesteric texture is modified, as soon as an external strain  $\lambda = \lambda_{xx}$  is applied. The director angle  $\phi$  is given by the formula:

$$\tan 2\phi = \frac{2\lambda^{1/4}(r-1)\sin 2\tilde{q}z}{(r-1)(\lambda^2 + \lambda^{-3/2})\cos 2\tilde{q}z + (r+1)(\lambda^2 - \lambda^{-3/2})}, \quad (1)$$

where  $\lambda$  stands for the imposed strain  $\lambda_{xx}$  and the parameter  $r$  is the intrinsic measure of local polymer chain anisotropy induced by the local uniaxial anisotropy of the mesophase (see [1] for detail). To simplify the results of [8], in the Eq. (1) we have approximated the transverse contraction  $\lambda_{zz}$  (due to the rubber incompressibility) by  $\lambda^{-1/4}$ , and the resulting affine contraction of the cholesteric pitch is taken into account by defining a reduced wave number  $\tilde{q} = \lambda^{1/4}q$ . Eq. (1) expresses the strain-induced bias of director orientations along the  $x$ -direction. The initially uniform helix coarsens continuously until a critical strain  $\lambda_c$  is reached, correspond-

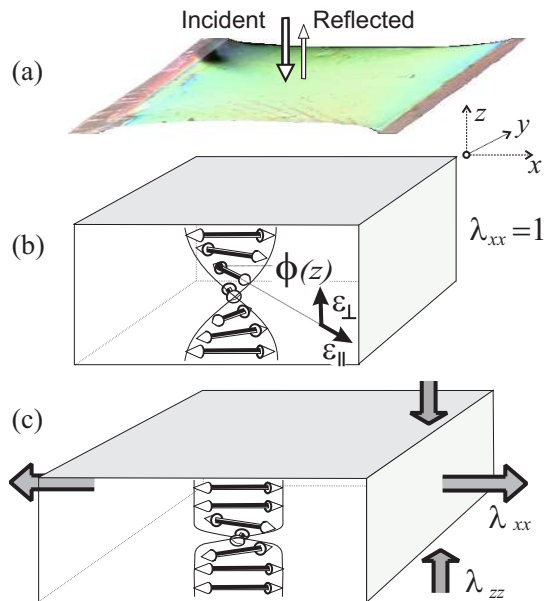


FIG. 1: (color online) (a) Photograph of a CLCE film, of size approximately  $1 \times 1 \text{ cm}^2$ , under small extension. The green color is given by selective reflection caused by the periodic structure. (b) Diagram sketching the CLCE geometry of a sample at rest,  $\lambda_{xx} = 1$ . At  $\lambda_{xx} = 1$  the cholesteric helical texture is characterized by a uniform director rotation about the pitch axis  $z$ . (c) Under uniaxial strain  $\lambda = \lambda_{xx}$  imposed along  $x$  the helical structure initially coarsens, leading to regions of faster and slower director rotation. The associated contraction of sample thickness is  $\lambda_{zz}$ . In all the experiments incident light is parallel to the pitch axis.

ing to the point of zero denominator in the right hand side of Eq. 1. At this point, the coarsened helical director texture discontinuously jumps into a non-helical state, modulated along  $z$ -axis but with the azimuthal angle  $\phi(z)$  not acquiring any phase, instead undulating back and forth about the  $x$ -direction. This behavior is shown in Figure 2. The critical strain can be easily estimated as  $\lambda_c = r^{2/7}$ , from Eq. (1). The parameter of backbone chain anisotropy,  $r$ , is the single parameter of the theory of ideal nematic (and cholesteric) elastomers;  $r = \ell_{\parallel}/\ell_{\perp}$  is interpreted as the average ratio of backbone chain step lengths along and perpendicular to the local director, or  $r = R_{\parallel}^2/R_{\perp}^2$  is the squared ratio of principal radii of polymer chain gyration. In nematic elastomers,  $r$  can be directly measured by examining the uniaxial expansion on cooling the elastomer, thus increasing the magnitude of the nematic order parameter. In a monodomain cholesteric rubber one can see a similar thermal phenomenon, represented as a uniform biaxial extension in the  $x$ - $y$  plane on cooling the CLCE, cf. Fig. 1. From such a measurement reported in [5] we can estimate that for this class of materials  $r \approx 1.16$ , leading to  $\lambda_c \simeq 1.04$  (that is, a critical strain of 4%). Recently much attention has been paid to evaluating and interpreting this parameter of anisotropic (locally uniaxial) networks [9, 10].

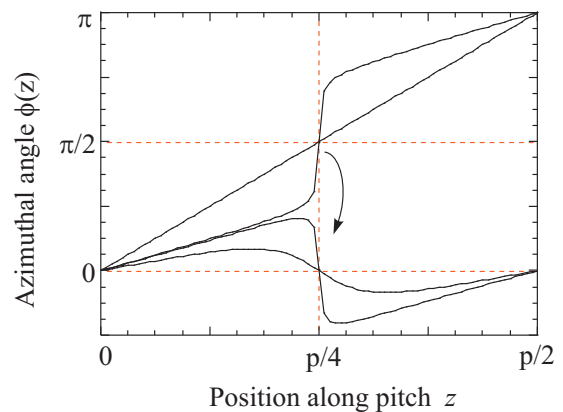


FIG. 2: The director distribution  $\phi$  inside the elastomer, calculated from Eq. (1). The initially uniform helix coarsens as the sample is strained, as indicated by the arrow. At a critical strain  $\lambda_c$  the texture becomes non-helical. See Ref. [8] for details.

Eq. (1) was tested in [7] and its key predictions have been verified. In particular, by measuring the non-trivial contraction in the  $z$ -direction it was seen that the deformation in the  $x$ -direction is, in fact, semi-soft. It was also confirmed that the average of director orientation under strain corresponds to the distribution expected from Eq. (1). The coarsening of the helix has been predicted to produce complex non-linear corrections to the optical response of the material, which are very different from the effect of an external field on a conventional cholesteric liquid phase [11, 12].

In this paper we study the rich optical properties of monodomain cholesteric elastomers. A range of samples is investigated that have been synthesized with stop-gaps across the visible range. We show how transmission and polarization of light can be controlled and manipulated through mechanical deformation of rubber films, by exploiting the coupling of the locally birefringent liquid crystalline texture to the underlying polymer network. We compare our results with the predictions of [11].

## II. METHODS

### A. Synthesis of materials

Free standing strips of single-crystal and well aligned cholesteric rubber have been prepared following the general principle suggested by Kim and Finkelmann [5]. A uniaxial deswelling is induced in a weakly crosslinked and swollen cholesteric gel, laterally constrained in a centrifuged film. The reduction of thickness while constraining the lateral dimensions is equivalent to a symmetric biaxial extension in the plane of the film. This leads to the macroscopic orientation of the director in the plane. Therefore, the helical axis is aligned perpendicular to the plane of the polymer film. This orientation is then locked

by completing a second-stage cross-linking of the rubbery network. We describe the materials in a reference system with the  $z$  axis parallel to the helical axis, as shown on the diagram in Fig. 1.

New side-chain cholesteric liquid crystal elastomers are synthesized in-house following the general method summarized above. Polysiloxane backbone chains are reacted with 90 mol% mesogenic side groups and 10 mol% of the two-functional crosslinker 1,4-di(11-undeceneoxy)benzene, labelled as 11UB in Fig. 3(a). The choice and the composition of mesogenic groups, see Fig. 3(a), is dictated by a number of considerations. First of all, we mixed two different nematogenic groups, 4-pentyloxyphenyl-4'-(4"-buteneoxy) benzoate (POBB) and 4-methoxyphenyl-4'-(4"-buteneoxy) benzoate (MBB), in equal proportion. This gives a strong nematic phase with no crystallization tendency and a low glass transition. The chirality is brought to the system by including the  $R(-)$  4-[(2-methyloctyl) benzoate]-4'-(4"-buteneoxy) benzoate (2MOB<sup>3</sup>) at different concentrations.

A word on terminology is due here. There are several ways of describing the chiral substances, developed in chemistry. The old Rosanoff (1906) notation distinguishes between D[+] (for *dextra*) and L[-] (for *laevo*) on the basis of relative arrangement of four different bonds of the chiral carbon. The Cahn-Ingold-Prelog (1956) notation is also based on ranking of bonds according to specific sequence rules, so that it can be used for more complex molecules; it specifies R[+] (for *rectus*, clockwise rotation) and S[-] (for *sinister*, anticlockwise). It is only natural, that different sources of organic chemistry data have mixed notations, e.g. the Aldrich catalogue quotes chiral molecules as R(-) and S(+). This simply reflects the fact that different chirality indices (scalar and tensorial) must be introduced to describe different physical responses, while the proper notation is not yet developed in spite of many recent advances [13, 14]. For instance, the sense of steric chirality (asymmetry in the geometric shape of the object) is not necessarily the same as that of the third-order dielectric polarizability  $\beta_{ijk}$  (determined by electronic structure) and that, in turn, may be different at different frequencies, for instance for the rotation of light polarization. The macroscopic "phase chirality" of cholesteric materials is a result of cooperative action of all such effects and is simply distinguished by the circular dichroism, so that a right-handed (clockwise, R\*) material reflects right-hand polarized light [2].

The technique of preparing monodomain cholesteric rubber requires that the crosslinking is carried out during slow de-swelling in the cholesteric phase and so it was essential that our mesogenic groups form the phase on their own – before polymerization. The mixture of the chosen monomers is a room-temperature cholesteric, achieving this purpose.

Materials with four different concentrations of chiral groups have been obtained, as shown in Fig. 3(a), with the molecular proportions 15, 20, 25 and 30%. The

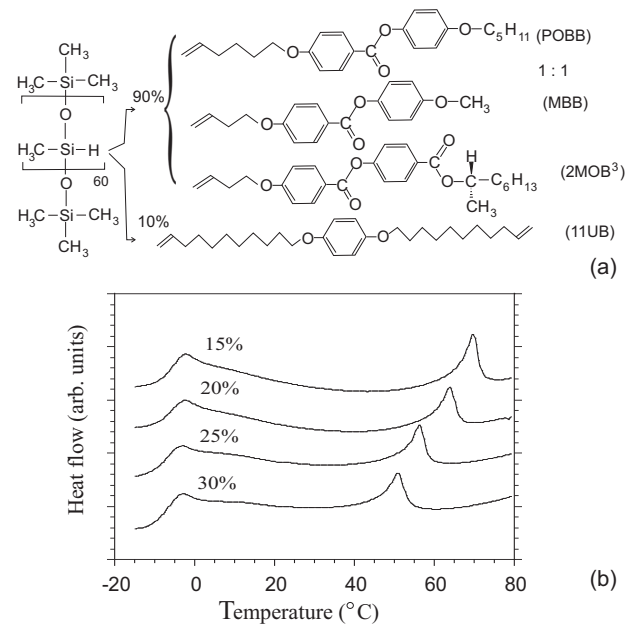


FIG. 3: (a) Chemical structures of the compounds forming the cholesteric elastomers under investigation. A siloxane backbone chain is reacted with 90 mol% mesogenic side groups and 10 mol% of the flexible di-functional crosslinking groups (11UB). The rod-like mesogenic (nematic) moieties are divided in the proportion 1:1 between POBB and MBB; the chiral  $R(-)$  rod-like moiety 2MOB<sup>3</sup> has been taken in the proportion of 15, 20, 25 and 30 mol% with respect to the nematic groups. (b) Differential scanning calorimetry results for the four materials studied in this work, indicating the nematic (cholesteric) clearing point and the glass transition variation with network composition.

hydrosilation reaction, with a platinum catalyst (from Wacker Chemie), was carried out under centrifugation at 7000rpm initially for 25 minutes at 75°C to form a partially crosslinked gel. For the further 8 hours the reaction proceeded under centrifugation at 30°C, during which time the solvent was allowed to evaporate, leading to an anisotropic deswelling of the gel and completion of crosslinking. All of the volume change in this centrifuge setup occurs by reducing the thickness of the gel, while keeping the lateral dimensions fixed. At the second-stage temperature of 30°C the dried gel is in the cholesteric phase and its director is forced to remain in the plane of stretching – this results in the uniform cholesteric texture sketched in Fig. 1. This kind of synthesis produces a very homogeneous strip of elastomer with the size of the order of 20cm×1cm×230μm.

Differential scanning calorimetry (DSC) was used to characterize the phase sequence of resulting elastomers (Perkin-Elmer Pyris 7 DSC). Figure 3(b) shows the typical scans on heating, indicating the glass transition temperature  $T_g \approx -7^\circ\text{C}$ , as is common for polysiloxane side-chain polymers. The clearing point, i.e. the isotropic-cholesteric transition temperature, clearly depends on the composition, decreasing from  $T_c \approx 65^\circ\text{C}$  for  $X=15\%$ ,

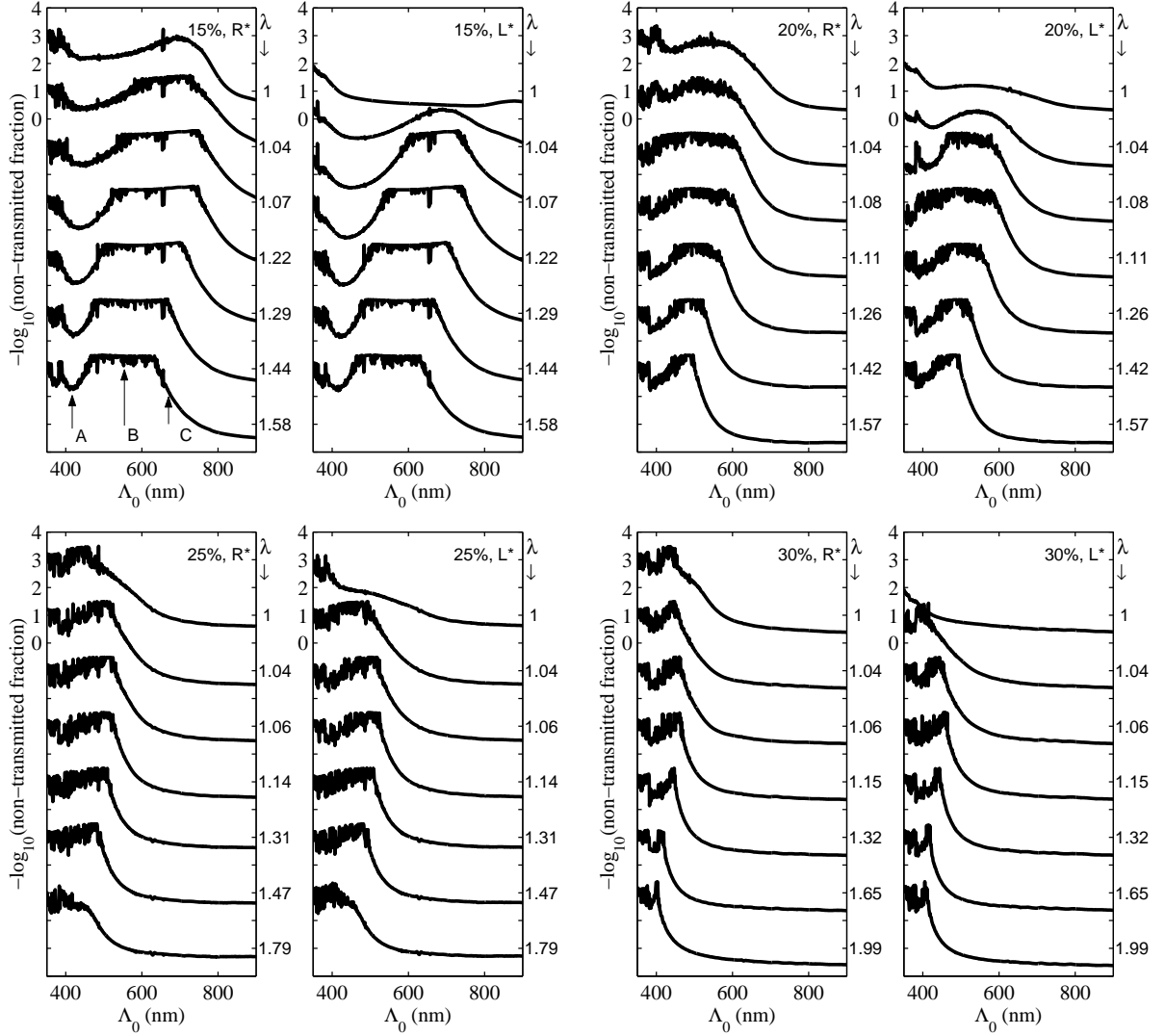


FIG. 4: Transmittance spectra for opposite circular polarizations through cholesteric elastomers with different fraction of chiral dopant: 15%, 20%, 25% and 30%. The circular polarizations and the concentration of chiral component are labelled in each panel. Each material is uniaxially strained by the amount  $\lambda_{xx} = \lambda$ , annotated beside the corresponding spectrum. Successive spectra are shifted downwards by 2 absorbance units for clarity. Flat regions of very low transmittance correspond to the detection sensitivity limit of the spectrometer. Three characteristic points are shown on the top-left panel and their evolution is discussed in the text. A: marks the minimum at low wavelength; B: marks the center of the reflection band; C: marks the point where the transmitted fraction is 0.01.

to  $T_c \approx 60^\circ\text{C}$  for 20%,  $T_c \approx 52^\circ\text{C}$  for 25% and to  $T_c \approx 46^\circ\text{C}$  for 30%. No additional phase transformations are found between  $T_c$  and  $T_g$ . All optical experiments are performed at room temperature, sufficiently far from both transitions.

## B. Experimental technique

Measurements of the transmitted fraction of circularly polarized light normally incident on the sample are made for wavelengths across the visible spectrum. A combination of a linear polarizer and a Fresnel rhomb is inserted

in the optical path of a HP-8453 UV/Vis spectrophotometer, so that the incident light reaches the sample having been circularly polarized. The clockwise R\* or anticlockwise L\* handedness of circular polarization is determined by the orientation of the linear polarizer. Light with a wavelength below  $\Lambda_0 \sim 320\text{nm}$  is not transmitted due to absorption in both the polarizer and the glass prism. For  $\Lambda_0 > 320\text{nm}$  the cholesteric materials under study reflect backwards the fraction of light that is not transmitted.

### III. PHOTONIC STOP-GAPS

The panels in Fig. 4 show the fraction of light transmitted by the cholesteric elastomers as a function of strain, for light of each circular polarization. We label right and left handed circularly polarized light by  $R^*$  and  $L^*$  respectively. These spectra are a measure of the photonic stop-gaps, and show the dramatic effect of mechanical deformation.

It is possible to make some observations which hold generally for the four materials under study. At no external strain ( $\lambda_{xx} = 1$ ) there is a very strong circular dichroism, the samples transmitting most of the  $L^*$  component of light but reflecting  $R^*$  for a range of wavelengths. The reflection peak, as expected, shifts into the blue (shorter cholesteric pitch) on increasing the proportion of chiral component in the material. As soon as a uniaxial strain is imposed, the transmitted intensity spectra for  $L^*$  polarized light show a continuous development of a new reflection gap, at the same wavelength as the intrinsic  $R^*$  peak. This dramatic change in the transmittance was first reported in [7] for another monodomain CLCE network. Now we can study this effect in much greater detail because our materials (especially the 15% and 20%) have a photonic gap centered at large wavelength. The development of a gap in the “opposite” circular polarization,  $L^*$ , even at a small strain, corresponds to the sudden onset of a bright coloring of the material, see Fig. 1. Indeed once the peak in  $L^*$  reflectance has fully developed, the sample reflects practically the totality of incident light at that wavelength. With further increasing uniaxial strain, the reflection gaps become more narrow and shift to lower wavelength. This corresponds to the change in color seen in stretched CLCE.

Above  $\lambda_{xx} \approx 1.1$  and above the  $R^*$  and  $L^*$  spectra are hardly distinguishable. This suggests that there is no macroscopic chirality left in the stretched cholesteric networks, which are apparently no longer twisted in a helical, albeit coarsened, fashion. We shall discuss this point below, making connection with optical rotation data and the state of stretched CLCE above the critical strain  $\lambda_c$ .

#### A. Effect of concentration of chiral dopant

Figure 5 shows the position of the stop-band edge as a function of the concentration of chiral moieties in equilibrium (at  $\lambda = 1$ ). As expected, the helix pitch  $p$  is tighter the higher the concentration  $X$  of chiral component. We find an excellent agreement with a relation

$$p = p_0 + c/X, \quad (2)$$

indicating that for low  $X$  each chiral molecular moiety induces chiral activity independently. For high  $X$ , the pitch tends to a saturation value  $p_0$ , which is a reflection of intrinsic chirality of the 2MOB<sup>3</sup> molecular group. For our materials, the fitting in Fig. 5 gives the values

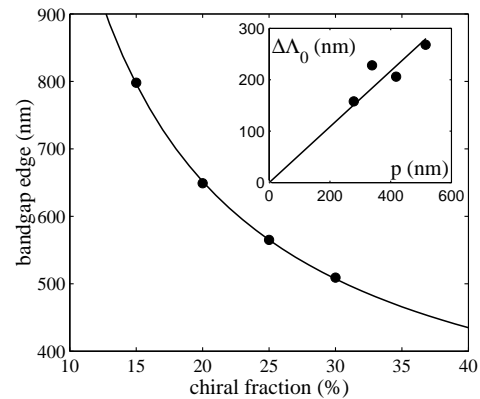


FIG. 5: Position of the bandgap edge as a function of the concentration  $X$  of chiral groups. The solid line is a fit to the Eq. (2). The inset shows the approximately linear dependence between the width of the bandgap,  $\Delta p$ , and the helical pitch itself. Here the solid line is a guide to the eye, indicating the proportionality  $\Delta\Lambda_0 \propto p$ .

$p_0 = 218\text{nm}$  and  $c = 8674\text{nm}$  (or  $86.7\text{nm}$  if  $X$  is more naturally expressed as a fraction, instead of a percentage). From this one could propose that if all side chains of our polymers were made of the chiral 2MOB<sup>3</sup>-group,  $X = 100\%$ , the resulting cholesteric would have a pitch of  $p \approx 295\text{nm}$ .

Figure 5 also shows the width of the stop-band as a function of the helical pitch wavelength. From the treatment of light propagation in an ideal cholesteric helix [2], a proportionality is expected between the bandgap width  $\Delta\Lambda_0$  and the pitch:

$$\Delta\Lambda_0 = p \frac{m_e - m_o}{\bar{m}}.$$

For the refractive indices  $m_e \simeq 1.75$  and  $m_o \simeq 1.6$  typical of thermotropic liquid crystals, the proportionality reads  $\Delta\Lambda_0 \simeq 0.1 p$ . For the CLCE materials we observe the expected proportionality, but the inset in Fig. 5 shows that the gap width is about 50% of the pitch, at least five times wider than in “classical” cholesteric liquid crystals. In addition, our separate measurements (not shown) of the evolution of transmission spectra with temperature (and, in consequence, with the nematic order parameter  $Q \propto m_e - m_o$ ) have indicated that the gap position and width change very little as one approaches the isotropic phase (although the amplitude of selective reflection does, of course, diminish). This means very likely that the pitch is not precisely single-valued throughout the elastomer thickness and the band width is determined by the quenched disorder inherent in the CLCE helix.

#### B. Effect of strain

Three characteristic points can be used to quantify the spectra shown in Fig. 4: the peak position (measured as

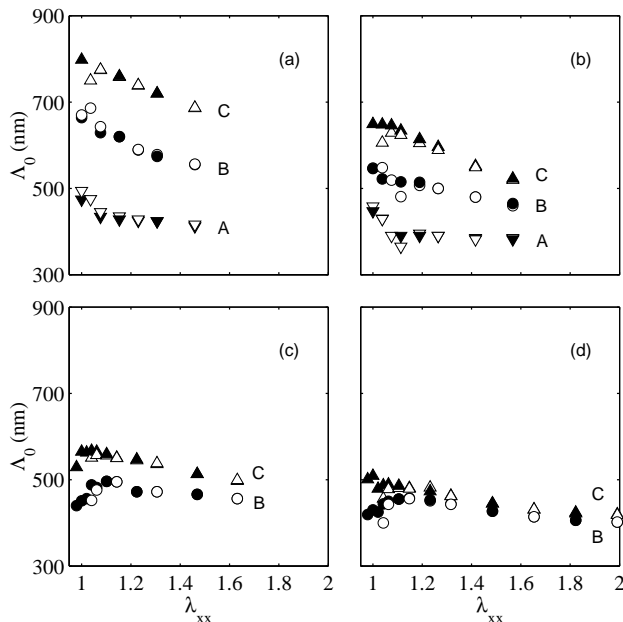


FIG. 6: The effect of uniaxial strain on the photonic stop-gap. A:( $\nabla$ ), B:( $\bullet$ ) and C:( $\blacktriangle$ ), correspond to the characteristic positions on the reflection peaks shown in Fig. 4. Solid symbols correspond to R\* circular polarization and empty symbols to L\*. The data are obtained from materials with different chiral dopant concentration X: (a) 15%, (b) 20%, (c) 25% and (d) 30%.

the center of the bandgap when the peak is at the detector saturation), the long wavelength band edge (measured at the half height of the reflection peak) and the center position of the trough between the primary reflection peak and the next rise at short (UV) wavelengths (only visible in 15 and 20% materials). The movement of each of these points is followed, as function of imposed strain, in Fig. 6. The plots show data for both the R\* and the L\* peaks but, of course, at very small strains  $\lambda < 1.1$  the L\* reflection peak has not yet developed to match the R\* gap. For large strains the gaps are indistinguishable, as the filled and open symbols in the plots indicate, and shift together towards smaller wavelengths.

It is also clear that the gap becomes narrower as a function of strain. There are two factors contributing to this. First of all, as we have seen in the previous section, the gap width is proportional to the pitch – which is affinely decreasing with the thickness of elastomer film (the middle data set in each of the four plots in Fig. 6). Secondly, and perhaps more importantly, the stretching of a cholesteric rubber film leads to some reduction in effect due to the quenched disorder, representing itself in the inhomogeneity of the local pitch as well as the wavering of its axis about  $z$ . The increasing external strain leads to greater alignment of the director in the sample plane and, as a result, to a greater perfection of the periodic texture. This is also the reason for increasing clarity of colors reflected from the material.

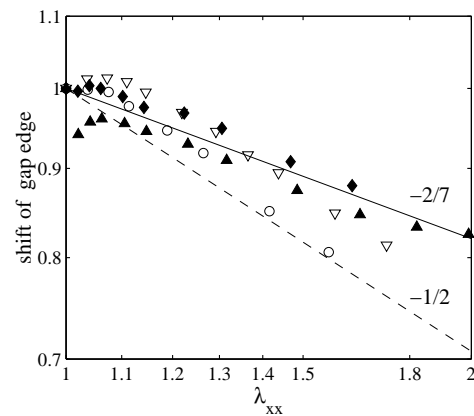


FIG. 7: Plot of the bandgap edge position relative to the value for the undeformed material, as function of strain, on a logarithmic scale. Symbols refer to materials with a different concentration of chiral dopant. ( $\blacktriangle$ ):X=30%, ( $\blacklozenge$ ):X=25%, ( $\circ$ ):X=20% and ( $\nabla$ ):X=15%. The lines correspond to two limiting scaling laws as described in the text.

The relative movement of the R\* reflection gap edges is shown in Fig. 7. The pitch of the cholesteric helix, which is probed by the lack of transmission of R\* light, is affinely deformed by the sample contraction along  $z$ -axis, and the shift of the reflection gap edge is a direct measure of this contraction,  $\lambda_{zz}$ . In an incompressible elastomer, an imposed extensional strain  $\lambda_{xx}$  induces a contraction in  $y$  and  $z$  directions. Figure 7 shows the scaling of the gap position as a function of strain. For an isotropic rubber one would always find a symmetric relationship:  $\lambda_{yy} = \lambda_{zz} = \lambda^{-1/2}$ . It can be clearly seen that the 30% and 25% samples follow a different scaling, the  $\lambda_{zz}$  strain following the power law  $\lambda_{xx}^{-2/7}$ . This is an expected result, predicted by semisoft elasticity of liquid crystal rubbers [1]. It occurs if the nematic director is allowed to rotate, as described by Eq. (1). Then, as explained in Refs. [8, 11], the rubber strip is effectively stiffer along the pitch axis and contracts much more in the plane of the director (along  $y$ -axis) and much less in its thickness:  $\lambda_{yy} = \lambda^{-5/7}$  and  $\lambda_{zz} = \lambda^{-2/7}$ .

However the 20% and 15% samples appear to follow the well known curve describing an isotropic rubber. We believe that this is due to an increased effect of disorder in the alignment of the director in the materials with a low chiral doping. The non-uniform alignment of helical pitch would also reflect in the large width of the bandgap as compared to an ideal helix. At present these effects are not considered in the theoretical description.

Additional bandgaps have been predicted [11, 12] to form under strain, at wavelengths which are around half of the original helical pitch. Their observation is difficult because they should appear close to our experimental limit of low wavelength, even for the 15% sample.

#### IV. CONCLUSIONS

We have presented experimental results showing the very rich optical behavior of monodomain cholesteric elastomers and studied the effects induced by mechanical deformation.

Such materials can be synthesized with optical stop-bands anywhere across the visible range. In analogy with a classical cholesteric liquid crystal, the undeformed samples exhibit a very strong circular dichroism, corresponding to a reflection band for light of circular polarization  $R^*$ , of the same helicity as the cholesteric structure itself. As soon as a uniaxial strain is imposed, a stop-band appears also for the opposite circular polarization  $L^*$  and the sample becomes an effectively one-dimensional broadband Bragg-grating, reflecting all light. The wavelength of the stop-gap is controlled by the external deformation. These properties were theoretically predicted in [8, 11] for an ideal material. However the extraordinary large width of the reflection band in all materials studied so far is a clear indication of imperfections in rubbery cholesteric networks. We believe a significant amount of quenched random disorder is inherent in these monodomain CLCE due to the preparation pro-

cedure, showing itself in both local variations of initial helical pitch  $p$  and the wavering of its axis. Both effects become suppressed on initial mechanical stretching in the plane of the director. This is in contrast with almost defect-free cholesteric networks that are prepared by densely crosslinking very thin cholesteric films spontaneously aligned by rubbed surfaces, such as those used in recent studies of low-threshold lasing [15].

To summarize, the present study confirms our understanding of the effects of a mechanical field on a cholesteric liquid crystal elastomer. These materials can be readily fabricated in large strips and have already found applications. Their surprisingly rich and well understood structural behavior will surely prove useful in novel photonic devices. Further theoretical investigation is required to describe the effects of quenched random disorder on the modulation of phase of the optical axis.

#### Acknowledgments

We thank Mark Warner for a number of useful discussions. This research has been supported by EPSRC.

- 
- [1] M. Warner and E. Terentjev, *Liquid Crystal Elastomers* (Clarendon Press, Oxford, 2003).
  - [2] P.-G. de Gennes and J. Prost, *The Physics of Liquid Crystals* (Oxford University Press, Oxford, 1994).
  - [3] V. Belyakov, V. Dmitrienko, and V. Orlov, *Sov. Phys. Uspekhi* **22**, 63 (1979).
  - [4] H. Finkelmann, H. Kock, and G. Rehage, *Macromol. Rapid Commun.* **2**, 317 (1981).
  - [5] S. Kim and H. Finkelmann, *Macromol. Rapid Commun.* **22**, 429 (2001).
  - [6] H. Finkelmann, S. T. Kim, A. Muñoz, P. Palffy-Muhoray, and B. Taheri, *Adv. Mater.* **13**, 1069 (2001).
  - [7] P. Cicuta, A. Tajbakhsh, and E. Terentjev, *Phys. Rev. E* **65**, 051704 (2002).
  - [8] M. Warner, E. Terentjev, R. Meyer, and Y. Mao, *Phys. Rev. Lett.* **85**, 2320 (2000).
  - [9] H. Finkelmann, A. Greve, and M. Warner, *Eur. Phys. J. E* **5**, 281 (2001).
  - [10] S. Clarke, A. Hotta, A. Tajbakhsh, and E. Terentjev, *Phys. Rev. E* **64**, 061702 (2001).
  - [11] P. Bermel and M. Warner, *Phys. Rev. E* **65**, 010702 (2002).
  - [12] P. Bermel and M. Warner, *Phys. Rev. E* **65**, 056614 (2002).
  - [13] M. Osipov, B. Pickup, and D. Dunmur, *Mol. Phys.* **84**, 1193 (1995).
  - [14] A. Harris, R. Kamien, and T. Lubensky, *Rev. Mod. Phys.* **71**, 1745 (1999).
  - [15] J. Schmidtke, W. Stille, and H. Finkelmann, *Phys. Rev. Lett.* **90**, 083902 (2003).